

Available online at [www.sciencedirect.com](http://www.sciencedirect.com)

ScienceDirect

journal homepage: [www.elsevier.com/locate/bbe](http://www.elsevier.com/locate/bbe)

## Original Research Article

# RASIT: Region shrinking based Accurate Segmentation of Inflammatory areas from Thermograms



Shawli Bardhan<sup>a</sup>, Mrinal Kanti Bhowmik<sup>a,\*</sup>, Tathagata Debnath<sup>a</sup>,  
Debotosh Bhattacharjee<sup>b</sup>

<sup>a</sup>Department of Computer Science and Engineering, Tripura University, Tripura, India

<sup>b</sup>Department of Computer Science and Engineering, Jadavpur University, West Bengal, India

## ARTICLE INFO

## Article history:

Received 23 March 2018

Received in revised form  
27 June 2018

Accepted 11 July 2018

Available online 03 August 2018

## Keywords:

Thermal imaging

Arthritis

Medical diagnosis

Image segmentation

RASIT

## ABSTRACT

Effective segmentation of thermal images reflecting the inflamed region in human body to assist medical diagnosis is a challenging task. In this paper we propose a method for thermal image segmentation, named as “Region shrinking based Accurate Segmentation of Inflammatory areas from Thermograms”, in short RASIT. The method comprising of four steps encompassing thermal image contextual electrostatic force extraction, intensity adjustment as applicable, automated generation of the weighted threshold, and segmentation of thermograms based on the computed threshold. The proposed method is operative devoid of the subjective and possibly questionable task of parameter selection clearly offering an edge over the state-of-the-art methods in terms of usage. The efficacy of our proposed technique is shown by experimenting on abnormal thermograms taken from two datasets: one is newly created knee arthritis thermogram dataset and another is online available Database of Mastology Research (DMR) of breast thermograms. The averages on correct detection rates obtained by the proposed method for both the knee and breast thermograms are 98.2% and 96.98% respectively with favorable inference on basis of Wilcoxon’s test. Application of the proposed method minimizes the complexity of parameter selection, time complexity of execution and amount of under segmentation compared to existing state-of-the-art methods of thermogram segmentation.

© 2018 Nalecz Institute of Biocybernetics and Biomedical Engineering of the Polish Academy of Sciences. Published by Elsevier B.V. All rights reserved.

\* Corresponding author at: Department of Computer Science and Engineering, Tripura University, Suryamaninagar 799022, Tripura, India.

E-mail addresses: [shawli.cse@gmail.com](mailto:shawli.cse@gmail.com) (S. Bardhan), [mrinalkantibhowmik@tripurauniv.in](mailto:mrinalkantibhowmik@tripurauniv.in) (M.K. Bhowmik), [tirtha.debnath@gmail.com](mailto:tirtha.debnath@gmail.com) (T. Debnath), [debotosh@ieee.org](mailto:debotosh@ieee.org) (D. Bhattacharjee).  
<https://doi.org/10.1016/j.bbe.2018.07.002>

0208-5216/© 2018 Nalecz Institute of Biocybernetics and Biomedical Engineering of the Polish Academy of Sciences. Published by Elsevier B.V. All rights reserved.

## 1. Introduction

Asymmetric inflammation in the human body is an indication of a pathological abnormality related to the internal anomaly. Image oriented recording of skin surface temperature distribution using thermal imaging under controlled environment, serves as the secondary temperature based diagnostic tool for abnormality detection [1]. Application of thermal imaging in inflammation oriented disease analysis is widely accepted in the diagnosis of arthritis-related joint disease [1,2] and breast abnormality detection [3,4]. Inflammation in joint with pain is a sign of arthritis in the human body and may lead to permanent damage of body structure. Arthritis mainly affects joints, bones, tendons, ligaments, and muscles. Certain rheumatic arthritis may also cause damage to internal organs. Common signs and symptoms of arthritis include pain, tenderness, stiffness, swelling etc. In the case of chronic arthritis (e.g. Rheumatoid arthritis), there is frequent exacerbation and remission of symptoms. Research shows that hundred different kinds of arthritis are present in the world and can affect persons of all age groups. The two most frequent types of arthritis are Rheumatoid Arthritis (RA) and Osteoarthritis (OA) [5]. The other frequently occurring types of arthritis affecting human body are Reactive Arthritis (ReA), Polyarthritis (PA), Monoarthritis (MA), Gouty arthritis (GA) etc. The present scenario in India shows that 15% of the total populations are suffering from arthritis [6] and in the US, 18% of the total disable persons are suffering from arthritis [7]. In India, the rate of prevalence of RA is almost 0.9% and this range is 0.5–1% worldwide [8–10]. Most of the popular methods of arthritis diagnosis and confirmation of inflammation comprise subjective evaluation and pathological tests. In the early stage of arthritis, subjective evaluation and laboratory tests may not be able to detect inflammation. The imaging modalities, like X-ray, Ultrasound and Magnetic Resonance Imaging (MRI) are also used for diagnosis of arthritis. But those modalities mainly identify the musculoskeletal changes of affected regions. In the initial stage of arthritis, as per the opinion of concerned medical experts, the musculoskeletal damage is insignificant and because of this, subjective evaluation does not provide any prominent impression of inflammation. As a result, detection of inflammation at this stage is difficult. In such situation, thermal imaging offers a supplementary, non-invasive as well as the non-radiating temperature specific inflammation viewing technique and used as decision-making modality for detection of inflammation generated from arthritis [1,2,10]. In the case of breast abnormality also, temperature pattern of breast thermogram is able to act as a secondary diagnostic tool. The presence of an abnormality in the breast tissue changes the normal temperature distribution in the breast region due to increase of metabolic activity. Non-radiating thermal imaging detects the abnormality in the temperature distribution by capturing the infrared radiation from the breast surface non-invasively [11]. Other substantial benefits of thermal imaging over non-invasive conventional inflamed area identification techniques are broad temperature spectrum, fast response time, reliability, high spatial resolution and safe approach for imaging oriented inspection of

inflammatory diseases [12]. The formation of a thermogram is purely dependent on the temperature distribution of the object or the skin surface of a human body which is photographed. It is established that nature of abnormality related to inflammation has got a strong reflection in terms of temperature distribution. Incidentally, manual identification of the inflamed area and its origin is a challenging proposition for a medical expert especially out of a large number of infrared (IR) images obtained from a huge population. Naturally, thermogram based automated segmentation of inflamed region is a very effective methodology supplementing manual diagnosis of the same by a medical expert. Assessment of the prognosis of treatment is also possible depending on monitoring the spread of the inflammation. In human body thermography, the inflamed region(s) consists of higher temperature compared to the background and other body regions. The inflamed region(s) is our region-of-interest (ROI) and represented by a set of higher gray level pixel intensities compared to the pixel intensities representing lower temperature regions of body in the thermogram. Due to the presence of low contrast and complexity in the background of thermogram [13], segmentation of the inflamed region(s) is a challenging task. Another important affecting factor in the segmentation of the inflamed region(s) in a thermogram is the blur effect produced due to the focusing error at the time of its acquisition. The blur effect also increases the complexity of thermogram segmentation. Other issues associated with segmentation are over-centralized intensity distribution, the presence of noise due to the limitation of the technology in acquisition system [13,14] and also for uncontrolled environmental factors.

In past research, authors applied popular segmentation methods for thermal image segmentation. The related works on thermogram segmentation have been summarized and given in Table 1. The state-of-the-art thermal image segmentation techniques as given in Table 1 shows the use of clustering, thresholding, region growing, and edge detection based segmentation of the ROI from the thermal image. Observation from the review indicates that the popular state-of-the-art segmentation methods suffers from the need of parameter selection depending on the type of thermograms.

Focusing on the shortcomings of existing techniques; we mainly concentrated on decreasing the load of parameter selection in our proposed inflamed region segmentation method from thermogram. The proposed method is described in the next subsection in brief.

### 1.1. Brief description of proposed method and contributions

In this paper, our aim is to develop an effective thermogram segmentation technique, inspired by the concept of Coulomb's Law of Electrostatic force on two static charges. We postulate that  $n$  pixels forming the input image may be considered as a closed system comprising  $n$  many static point charges. The electrostatic force of any individual pixel may be defined as the impact of all other first order neighborhood pixels on that individual pixel in the image ignoring the effect of self-influence. The electrostatic force from the neighborhood

**Table 1 – Related work of thermogram segmentation.**

Segmentation techniques	Method used	Demerits associated with inflamed ROI segmentation from thermogram
Clustering based segmentation	Fuzzy C-means (FCM) [2,15,16], K-means [16,17,18], Expectation Maximization (EM) [2,19], Particle Swarm Optimization based FCM clustering [20], Swarm optimization-based algorithms [21].	Cluster number initialization, cluster center initialization, selection of the cluster which represents the inflamed region from clustering output.
Threshold based segmentation	Otsu thresholding [12,22,23], Minimum Error Thresholding (MET) [12], Kapur thresholding [12], Hamadani determined thresholding [12].	Threshold value selection.
Region growing based segmentation	Threshold based region growing [24,25]	Manual selection of multiple seed points, selection of the stopping parameter related to grouping the pixels.
Edge detection based segmentation	Gradient based edge detection [23], level set method combined with manual seed selection [26], improved region based level set method [16], sobel edge detection method [24].	Due to the lack of boundary sharpness of thermal images, edge detection is not able to detect the boundary of an inflamed region in the thermogram or too many edges are detected due to the intensity variation of thermal image.

pixels minimizes the intensity of the surrounding background region of the inflammatory (hot) region of interest (ROI) towards minimum gray intensity level with the progress in the number of iterations. The outcome of the step is further divided into foreground and background regions in respect of a threshold value determined in an automated manner. The proposed method follows the region shrinking mechanism of ROI because of the use of automated thresholding. To ensure minimization, but not the elimination of ROI, an appropriate choice of stopping criteria needs to be worked out. The RASIT minimizes the difficulties of parameter selection and accurate segmentation with a minimum rate of cumulative over and under segmentation.

The performance of the proposed method is evaluated with the existing state-of-the-art segmentation techniques based on the ground truth prepared by the experts for knee thermogram dataset and online available existing breast thermogram dataset. In summary, the main contributory works of the paper includes:

- a) The proposed Region Shrinking Segmentation method (RASIT) performs optimal segmentation of inflamed ROI (s) with a minimum requirement of parameter selection.
- b) The execution time of the proposed method is less for inflamed region extraction compared to cluster- and threshold-based state-of-the-art methods.
- c) The proposed method minimizes under segmentation compared to the state-of-the-art cluster- and threshold-based methods.
- d) The inflammation oriented validation of knee thermogram dataset has been performed through pathological and subjective evaluations of the diseases.

The remaining paper is organized as follows: Section 2 contains a detailed description of the Electrostatic Force for

Segmentation. Section 3 describes the Region shrinking based accurate segmentation of inflammatory areas from thermograms. Section 4 explains dataset collection and ground truth generation. Sections 5 and 6 contain the results and discussion respectively. Finally, the conclusion and future work are presented in Section 7.

## 2. Electrostatic force based segmentation (EFS)

The objective of the proposed region shrinking based segmentation technique is to extract the ROI from thermograms. Region shrinking is a procedure that identifies the pixels having similar properties, from an image, based on predefined criteria. The basic approach is to start with the entire image and shrink it toward the area specified by the predefined criteria.

Our proposed Electrostatic Force based Segmentation (EFS) technique, segments the inflamed ROI by shrinking the input thermogram iteratively. EFS is inspired from the electrostatic force defined in the Coulomb's Law of Electrostatic. It is important to note that the electrostatic force and the force used in EFS are similar, but not the same. Although the electrostatic force has both magnitude and direction, in this work, we have considered only the magnitude of the force acting upon the image pixels. To explain the concept of EFS, in the rest of the section, we discuss the Coulomb's Law of Electrostatic and draw a relationship between the Coulomb's Law of Electrostatics and EFS.

### 2.1. Coulomb's Law of Electrostatics

The Coulomb's Law of Electrostatic formalizes the interaction between two static point charges. Considering, two points A and B having charges  $q_A$  and  $q_B$  respectively, maintaining a

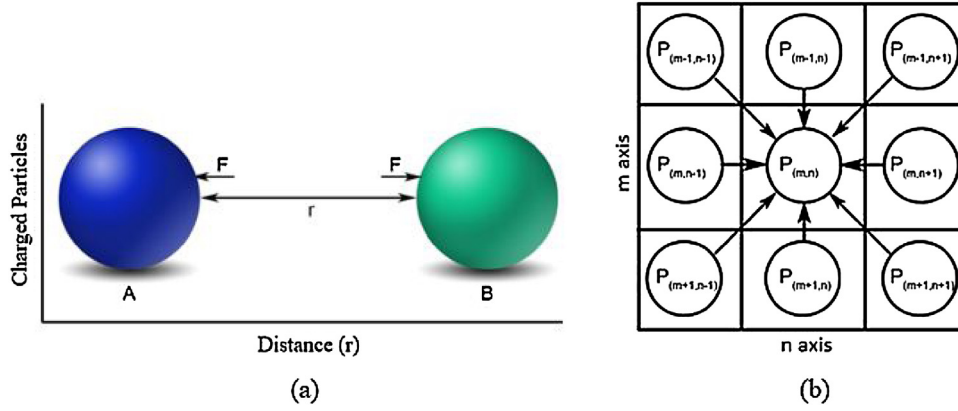


**Fig. 1 – (a) Electrostatic force between two charged particles A and B; (b) Image Contextual Electrostatic Force on a pixel from its 8-neighborhood pixels.**

distance  $r_{AB}$  between one another, as shown in Fig. 1(a), Coulomb's electrostatic force ( $F$ ) is given by:

$$F_{AB} = \frac{K \times q_A \times q_B}{r_{AB}^2} \quad (1)$$

here  $K$  is the Coulomb's Electrostatic constant. When cumulated over  $n$  point charges, the corresponding force  $F_i$  exerted on an arbitrary point charge  $q_i$   $\{q_i, 1 \leq i \leq n\}$  will be:

$$F_i = \sum_{\substack{j=1 \\ i \neq j}}^n \frac{K \times q_i \times q_j}{r_{ij}^2} \quad (2)$$

here  $r_{ij}$  is the distance between  $q_i$  and  $q_j$  charges.

## 2.2. Electrostatic force image (EFI)

Drawing inspiration from Coulomb's Law of Electrostatic force applicable to static charge particles, we, in the present context, formulate a theoretical framework appropriate for pixels forming an image. As per this framework, based on Eq. 1, two pixels A and B having intensity  $P_A$  and  $P_B$  maintaining distance  $r_{AB}$  from each other will interact through a force  $F_{AB}$  as:

$$F_{AB} = \frac{K \times P_A \times P_B}{r_{AB}^2} \quad (3)$$

In Coulomb's Law, the value of constant  $K$  is  $9 \times 10^9 \text{ N m}^2/\text{C}^2$ . For a gray scale image, we considered  $K$  as 255 which is the highest intensity level in the gray scale image. Considering the coordinates of the participating pixels A and B as  $(x_A, y_A)$  and  $(x_B, y_B)$  respectively, the Euclidian distance between them is:

$$r_{AB} = \sqrt{(x_A - x_B)^2 + (y_A - y_B)^2} \quad (4)$$

The resemblance between Coulomb's Law of Electrostatic force in respect of a pair of static charge particles as presented in Eq. 1 vis-a-vis that in respect of a pair of pixels participating in an image as per Eq. 3 is understandable.

The cumulative force exerted on a pixel from its first order neighborhood pixels (8-neighborhood) is calculated for every pixel in the image, represented by Eq. 5 and demonstrated in Fig. 1(b).

$$F_{(m,n)} = \sum_{\substack{x=m-1 \\ (x,y) \neq (m,n)}}^{m+1} \sum_{y=n-1}^{n+1} \frac{K \times P_{(m,n)} \times P_{(x,y)}}{r^2} \quad (5)$$

here  $P$  is an image of size  $X \times Y$  and  $P_{(m,n)}$  is the intensity of the candidate pixel on which the Electrostatic Force (EF) is calculated.  $P_{(x,y)}$  represents the  $(x,y)^{\text{th}}$  neighbor of  $P_{(m,n)}$ , where  $x \in \{m-1, m, m+1\}$  and  $y \in \{n-1, n, n+1\}$   $r$  is the Euclidian distance between  $P_{(m,n)}$  and  $P_{(x,y)}$  calculated similar to Eq. 4.  $F$  is the computed Electrostatic Force Image (EFI).

While obtaining the cumulative force on an individual pixel as per Eq. 5, intensity adjustment based on input intensity range may be needed in the event of accumulation of large value. Intensity adjustment is done by following linear interpolation as per Eq. 6.

$$J_{(m,n)} = \left( \frac{(P_{(i,j)}^{\max} - P_{(i,j)}^{\min})}{(F_{(i,j)}^{\max} - F_{(i,j)}^{\min})} * (F_{(m,n)} - P_{(i,j)}^{\min}) \right) + P_{(i,j)}^{\min} \quad (6)$$

here  $P_{(i,j)}^{\max}$  and  $P_{(i,j)}^{\min}$  are the maximum and minimum intensity values present in the input image,  $P$  respectively. Similarly,  $F_{(i,j)}^{\max}$  and  $F_{(i,j)}^{\min}$  indicate maximum value and minimum value present in the EFI matrix,  $F$  respectively. After intensity adjustment, the output is stored in the  $(m, n)^{\text{th}}$  coordinate of the image  $J$  for the corresponding  $F_{(m,n)}$ . Here,  $J$  is the intensity adjusted output of EFI computation. The EFI computation and intensity adjustment of the same is done iteratively as shown in Fig. 2.

Since EFI is an iterative process, it consists of the possibility of diminishing the foreground region with the

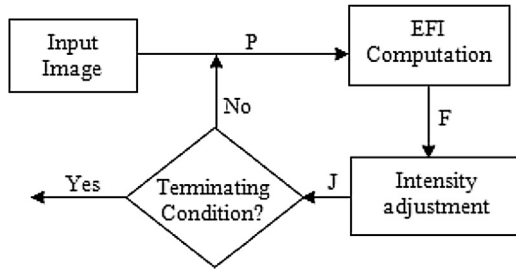


Fig. 2 – Iterative improvement of EFI for segmentation.

progress of iterations. Therefore, EFI based ROI segmentation suffers from the issue of selecting terminating condition. To determine the terminating condition, an automatic threshold selection process has been introduced. The complete segmentation algorithm along with terminating condition and automatic threshold selection is discussed in the next section.

### 3. Region shrinking based Accurate Segmentation of Inflammatory areas from Thermograms (RASIT)

The Region shrinking based Accurate Segmentation of Inflammatory areas from Thermograms (RASIT) mainly aims to segment the inflamed ROI from the thermal images using EFI. Fig. 3 shows the flow diagram of RASIT method for segmenting inflamed region from a knee thermogram.

#### 3.1. Preprocessing of the thermograms

The knee and the breast thermograms used for segmentation are stored following the gray palette color representation format. In this palette, the relation between temperature and pixel intensity is proportional to each other. The 24-bit gray palette consists of the Red (R), Green (G) and Blue (B) channels. The values of R,G and B channels for any pixel is equal to each other and this characteristic is responsible for visually gray representation of thermogram with 24-bit. Therefore, for 8 bit representation, selection of any of the channel will represent the whole image without losing the pixel properties of original thermogram as the

8-bit representation is identical with any of the R, G, B channels of the image. In our analysis, we choose the first channel, i.e. R channel of the image for 8 bit representation of the input data. The captured thermograms also consist of temperature scale, labels, and tags. Thus, for proper extraction of the inflamed region through the RASIT method, the knee, and the chest regions are manually cropped. Manually extraction of important region decreases the processing time of segmentation techniques.

#### 3.2. RASIT algorithm

The input of the RASIT algorithm is a gray scale thermogram  $I$  of size  $x \times y$ . The  $I$  is stored in  $R$ . Here  $R$  is a copy of  $I$  used for processing within the algorithm keeping the input image ( $I$ ) unchanged.  $\Phi_{Old}$  and  $\Phi_{New}$  are the threshold values from the previous and current step respectively, having initial value as 0. The stopping condition,  $\mu$ , and the loop condition variable  $COND$ , are set to 2 and 0 respectively. Termination of RASIT method is performed with the updation of  $COND$  from 0 to 1. The variable  $P$  is initialized with  $R$  and  $R$  is normalized by dividing with 255 and stored into another variable  $P$  for the convenience of algorithm processing. The value of  $R$  would change in successive iterations. The EFI is computed considering each pixel of the image  $P_{x \times y}$  using Eqs. 5 and 6 and as a result an image  $J_{x \times y}$  is generated.

The stopping criteria of RASIT algorithm depends on the automatically generated threshold value. The threshold  $\Phi_{New}$  changes dynamically in each iteration according to the image  $J$ . It is calculated automatically using the weighted average of the intensities present in the image by following Eq. 7.

$$\Phi_{New} = \frac{\sum_{i=0}^{255} i \times h(i)}{\sum_{i=0}^{255} h(i)} \tag{7}$$

here  $i$  represents the intensity of a pixel and  $h(i)$  is the number of occurrences of that intensity value in the image. This value of the threshold  $\Phi_{New}$  is used to generate a binary mask  $\eta$ , by using Eq. 8.

$$\eta_{(m,n)} = \begin{cases} 1 & \text{if } J_{(m,n)} > \Phi_{New} \\ 0 & \text{if } J_{(m,n)} \leq \Phi_{New} \end{cases} \tag{8}$$

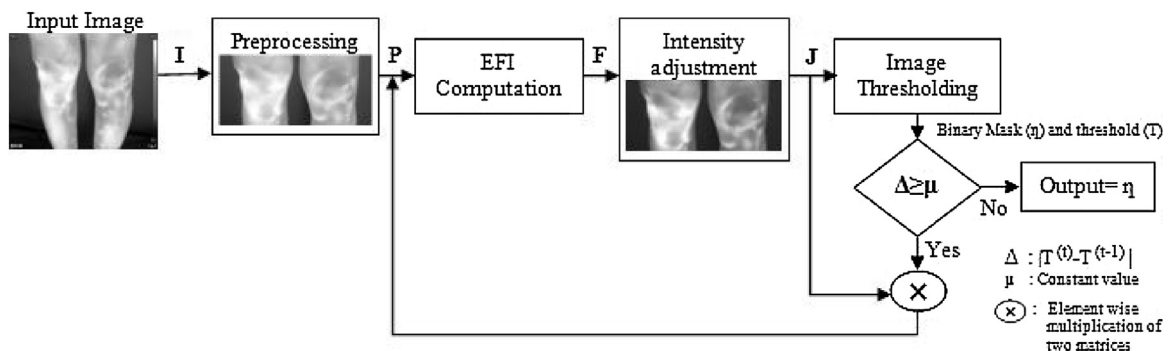


Fig. 3 – Flow diagram of Region shrinking based Accurate Segmentation of Inflammatory areas from a knee thermogram.

Algorithm 1: The RASIT Algorithm.

```

Input:  $I_{x \times y}$ 
Initialize:  $R \leftarrow I$ ,  $\Phi_{Old} \leftarrow 0$ ,  $\mu \leftarrow 2$ ,  $\Phi_{New} \leftarrow 0$ ,  $COND \leftarrow 0$ 
1.   while  $COND \neq 1$ 
2.      $P' \leftarrow R, P \leftarrow R/255$ 
3.      $F \leftarrow$  EFI matrix generation from  $P$  using Eq. 5
4.      $J \leftarrow$  Intensity adjusted output of  $F$  using  $P'$  and Eq. 6
5.      $\Phi_{New} \leftarrow$  New threshold from  $J$  using Eq. 7
6.      $\eta \leftarrow$  Binary Mask generation from  $J$  using
       threshold  $\Phi_{New}$  by following Eq. 8
7.      $R \leftarrow$  ROI extraction from  $J$  using  $\eta$  and Eq. 9
8.      $\Delta \leftarrow | \Phi_{Old} - \Phi_{New} |$ 
9.     if  $\Delta \geq \mu$ 
10.       $COND \leftarrow 0$ 
11.    else
12.       $COND \leftarrow 1$ 
13.    end if
14.     $\Phi_{Old} \leftarrow \Phi_{New}$ 
15.  end while
16.   $\Psi = I \otimes \eta$ 

Output:  $\Psi$ 

```

In successive iteration, the value of  $\Phi_{New}$  dynamically changes and because of that, the binary mask  $\eta_{x \times y}$  is also changed accordingly. The purpose of creating the binary mask  $\eta_{x \times y}$  is to extract the ROI from  $J_{x \times y}$ . The extracted ROI in successive iteration is stored in the matrix  $R_{x \times y}$  using the Eq. 9 by element-wise multiplication of intensity adjusted EFI ( $J_{x \times y}$ ) and binary mask ( $\eta_{x \times y}$ ).

$$R_{(m,n)} = J_{(m,n)} \otimes \eta_{(m,n)} \quad (9)$$

As an outcome of Eq. 9, the pixels with intensity greater than  $\Phi_{New}$  of the image  $J$  will remain in the image  $R$ , as they are probably included in the ROI.

In each iteration, the stopping condition of RASIT algorithm has been performed by checking the absolute difference ( $\Delta$ ) in between threshold value of previous iteration and present iteration ( $\Phi_{Old}$  and  $\Phi_{new}$ ) as given in Algorithm 1. Minor difference implies that the RASIT is approaching toward its saturation point. Therefore, the algorithm continues until the value of  $\Delta$  remains greater than a minimum value  $\mu$ , which is a constant. The value of the constant is discussed in Section 6.1. In the case of  $\Delta \geq \mu$ , the variable  $COND$  is set to 0 and the iterative process will continue. Therefore, termination of iteration is performed by rejecting the condition, which will set  $COND$  as 1 as shown in RASIT algorithm. Finally, the ROI ( $\Psi$ ) from the input image is generated by following Eq. 10.

$$\Psi_{(x \times y)} = I_{(x \times y)} \otimes \eta_{(x \times y)} \quad (10)$$

### 3.3. Proposed method (RASIT) as region shrinking model for image segmentation

The shrinking property defined in descriptive set theory is dependent on the Universal Class and disjoint sets [27]. The concept of descriptive set theory based region shrinking may be applied for image segmentation if the iterative process outcome follows shrinking property.

**Definition 1.** An image  $I$  has the shrinking property if the output of segmentation ( $S$ ) at  $k^{\text{th}}$  iteration over  $I$  is such that:

$$S^1(m, n) \supset S^2(m, n) \supset \dots \supset S^k = S^{k+1} \quad (11)$$

here  $S^1 = I$  and  $I$  is an  $M \times N$  image. The shrinking method for image terminates when two consecutive outputs (at the  $k^{\text{th}}$  step and  $(k+1)^{\text{th}}$  step) are same. Comparing with descriptive set theory based shrinking property [27],  $S^k$  is considered here as the Super class which contains a single set  $S^{k+1}$  such that  $S^k \supset S^{k+1}$ .

**Theorem 1.** Proposed method follows region shrinking model for segmentation

**Proof.** As discussed in the RASIT algorithm, the effect of the EF extraction process on a pixel ( $P_{(m,n)}$ ) depends on its neighborhood ( $P_{(x,y)}$ ) for EFI generation, as:

$$\text{Case 1: If } \forall P_{(x,y)}^k > P_{(m,n)}^k \text{ then } J_{(m,n)}^k > P_{(m,n)}^k$$

$$\text{Case 2: If } \forall P_{(x,y)}^k = P_{(m,n)}^k \text{ then } J_{(m,n)}^k > P_{(m,n)}^k$$

$$\text{Case 3: If } \forall P_{(x,y)}^k \approx P_{(m,n)}^k \text{ then } J_{(m,n)}^k > P_{(m,n)}^k \text{ or } J_{(m,n)}^k \leq P_{(m,n)}^k$$

$$\text{Case 4: If } \forall P_{(x,y)}^k < P_{(m,n)}^k \text{ then } J_{(m,n)}^k < P_{(m,n)}^k$$

$$\text{Case 5: If } \exists P_{(x,y)}^k \mid P_{(x,y)}^k < P_{(m,n)}^k \text{ then } J_{(m,n)}^k \leq P_{(m,n)}^k$$

From the above cases, it is clear that if case 1 exists then case 5 also exists. Therefore, except case 2, all  $J_{(m,n)}$  tends to zero with the progress of iteration number,  $k$ . Since the variation in intensity distribution is present in all the input images, so with the increase of the iteration number, the background pixels affect the intensity of uniform region as EFI outcome. The edge pixels of the  $3 \times 3$  uniform region is firstly affected by the non-uniform neighbourhood pixels by following Eq. 5. As the  $3 \times 3$  neighbourhood of each pixels of the  $3 \times 3$  uniform region are not always similar to each other, so the outcome of Eq. 5 for all pixels are also not identical. After  $k^{\text{th}}$  step, EFI converts the intensity distribution of a uniform region to non-uniform region and  $\forall P_{(x,y)}^k \neq P_{(m,n)}^k$  will occur. Therefore, case 2 will never occur in a consistent manner for all the iterations of EFI computation. This will only happen when all the pixels of an image have same value, which is not at all possible for a real life image.

Due to the presence of cases 3-5 in gray palette thermal image, the number of pixels with intensity value as 0 will also increase with the increase of iteration. After a certain number of iterations, say  $(k+1)$ , the output will become identical with EFI output at  $k^{\text{th}}$  iteration. The iteration based output ( $C_{(m,n)}^k$ ) of RASIT can be represented by Eq. 12 to Eq. 14.

$$C_{(m,n)}^1 = \{J_{(m,n)}^1\} \mid J_{(m,n)}^1 > \Phi^1 \quad (12)$$

$$C_{(m,n)}^k = \{J_{(m,n)}^{k-1}\} \mid J_{(m,n)}^{k-1} > \Phi^{k-1} \quad (13)$$

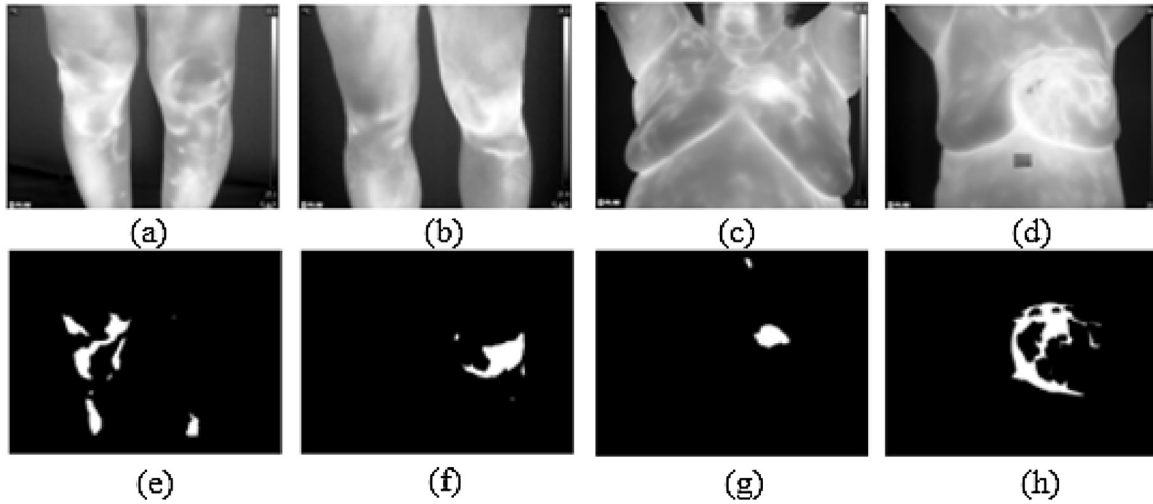


**Fig. 4 – (a, b) Captured thermograms related to knee arthritis; (c, d) Collected thermograms related to breast abnormality from DMR dataset; (e–h) Binary ground truth images related to the inflamed region of interest(s) corresponding to the thermograms given in (a)–(d) respectively.**

$$C_{(m,n)}^{k+1} = \{J_{(m,n)}^k\} | J_{(m,n)}^k > \Phi^k \tag{14}$$

The relationship between outputs of successive iterations can be given by Eq. 15 to Eq. 18, which establishes the shrinking model given in Definition 1.

$$C_{(m,n)}^1 = P^{(m,n)} \tag{15}$$

$$C_{(m,n)}^1 \supset C_{(m,n)}^2 \tag{16}$$

$$C_{(m,n)}^{k-1} \supset C_{(m,n)}^k \tag{17}$$

$$C_{(m,n)}^k = C_{(m,n)}^{k+1} \tag{18}$$

## 4. Dataset description and ground truth generation

### 4.1. Dataset description

The RASIT is tested over the thermograms of bilateral knee joints and breast regions. The frontal knee thermograms are collected from patients who have knee arthritis under the supervision of a medical expert and by following standardized protocols of acquisition [10]. The first row of Fig. 4 shows the samples of the knee and breast thermograms. All the knee and breast thermograms consist of inflamed region(s). Validation and ground truth generation of the inflamed region(s) from Medical Infrared Thermogram (MIT) related to inflammatory pain is a complex task. In our captured dataset, the validation has been performed with the help of a medical expert. In the case of breast thermograms, all the gray palette thermograms of the sick

patients are collected from existing DMR (Database of Mastology Research) database [28]. The rest of the section describes validation and ground truth generation of the captured dataset.

#### 4.1.1. Validation of knee inflammation

Inflammation in the human body is a sign of abnormality. In the case of arthritis, the severity of the disease can be determined by medical experts based on the subjective evaluation of inflammation. However, inflammation may occur in body joints due to fracture or for other abnormalities, environmental condition, and external pressure in knee joints. Based on this issue, we controlled the environmental conditions by the selection of proper acquisition protocols [10]. Moreover, the validation of inflammation of the thermograms of our dataset clarifies that the inflammation present in the knee joints is due to arthritis. The validation is performed by following two parameters: subjective evaluation, and clinical test, as described below.

*Subjective evaluation:* Subjective evaluation of inflammation related to arthritis in knee joints are performed by medical experts. The evaluation is executed depending on tenderness (T), swelling (S), redness (R), and restriction of movement (ROM) together or presence of synovitis (Syn). The presence of synovitis directly indicates the presence of inflammation due to arthritis. In the other cases, inflammation is confirmed if two of the other factors (T, S, R, and ROM) are present in the knee joint. Based on subjective evaluations of arthritis, the statistics of the factors with intensity (mild, moderate and severe) is given in Table 2, and confirms the presence of arthritic inflammation in the knee thermograms.

*Clinical test:* To confirm inflammation in the knee region, the Erythrocyte Sedimentation Rate (ESR) is calculated for all the patients. In the case of inflammatory arthritis, the ESR rate increases. The normal range of ESR is 0–15 mm/h for male and 0–22 mm/h for female [29]. The range of ESR for all the patients whose thermograms are used in our analysis is above 25 mm/h.

**Table 2 – Statistics of subjective evaluation of knee inflammation.**

Factors for subjective evaluation	No. of thermogram	Intensity of factors		
		Mild	Moderate	Severe
Tenderness	33	9	15	9
Swelling	26	5	14	7
Redness	2	2	0	0
Restriction of Movement	18	6	7	5
Synovitis	8	5	1	2

#### 4.2. Ground truth generation

The goal of the ground truth generation of the datasets is to validate the RASIT algorithm as well as to perform a comparison of the proposed method with the existing state-of-the-art techniques. Manual segmentation by an expert is the most commonly used technique to compute the ground truths. However, manual segmentation by a single expert may lead to erroneous result due to the expert's biases, boredom, and fatigue. Hence, multiple manual segmentations were performed on thermograms by different technicians for ground truth generation. For a single thermogram, five sets of segmentation results were generated by five individual technicians using the GNU Image Manipulation Program (GIMP) [30] software. The inflamed region represented by higher gray level pixels in the thermogram is considered as the foreground object and the rest as background. The foreground pixels are represented as white pixels (intensity value 1) and the background is converted into the black (intensity value 0). From the multiple ground truths generated by technicians for a single knee thermogram, the absolute ground truth is finalized based on the voting policy and evaluation by a medical expert. The voting policy is based on the threshold value,  $k$ . The value of  $k$  for  $i^{\text{th}}$  pixel determines whether the pixel is considered as a foreground pixel or not. The variable  $k$  is defined as  $k = (j + 1)/2$ , where,  $j$  indicates the total number of ground truths generated by technicians. The  $i^{\text{th}}$  pixel is considered as foreground pixel in the final ground truth if at least  $k$  number of technicians included it as a foreground pixel. The medical expert ultimately validates the final ground truth of knee thermogram depending on the clinical findings. The rejected ground truths are regenerated under the supervision of the medical expert by following the above mentioned procedure. The (e) and (f) images of Fig. 4 show examples of the final ground truths of corresponding knee thermograms given in the (a) and (b) of Fig. 4. In the case of breast thermograms also the ground truth for the inflamed regions is generated through voting policy as described above. The examples of generated ground truths for breast thermograms of Fig.4(c) and (d) are shown in Fig. 4(g) and (h) correspondingly.

## 5. Experimental results

The experiment has been performed over 50 arthritis affected knee thermograms and 44 breast thermograms of breast

abnormality related sick patients. The acquisition and collection of thermograms are described in the previous section. In this section, we present experimental results illustrating the ability of the proposed method on segmenting inflamed regions from thermograms comparing with state of the art techniques. The measurement of the ability of accurate segmentation is performed based on quantitative evaluations of segmentation output with ground truth data and statistical significance analysis of the measuring factors as described in the rest of the section.

#### 5.1. Quantitative and qualitative analysis based comparative study

In our comparative study, the area of the segmented region is compared with the area of the ground truth region for performance analysis of the segmentation techniques. The outcome of the segmentation techniques and generated ground truths are converted into binary images, where the inflamed region(s) is represented by white pixels with intensity value 1 and background region is represented through black pixels with intensity value 0. The quantitative analysis of area/boundary is performed by the intensity-based similarity measurement over the binary mask of ground truth, and segmented ROI generated through existing and proposed RASIT method. The pixel oriented Simple Matching Coefficient based similarity measurement in between ground truth and the segmented output is the popular method of area based performance analysis. These measurements mainly depend on True Positive (TP), False Positive (FP), True Negative (TN) and False Negative (FN) values. The estimated summary of TP, FP, TN, and FN is given in Fig. 5 using binary values (0 and 1). Using the above mentioned units (TP, FP, TN, and FN), we calculated Dice's Similarity coefficient (DSC), Accuracy (ACC) and Sensitivity (SENS) for the evaluation of the segmentation methods presented here. The maximum value of DSC, ACC, SENS indicates better segmentation output. The performance of segmentation techniques also may suffer from over and under segmentation. So, the quality of segmentation was measured by amount of Over segmentation (OSeg) and Under-segmentation (USeg) as used by Belgiu et al. [32]. In the case of over-segmentation, multiple segmentation of a single region occurs, and under-segmentation generates an insufficient segmentation of multiple regions. So, in the case of over-segmentation, the output of segmentation becomes smaller than the ground truth region and the vice versa happens through under-segmentation. Collectively both the over and under-segmentation causes erroneous output compared to

		Segmentation Output	
		1	0
Ground Truth	1	TP	FN
	0	FP	TN

Fig. 5 – Summary of measuring unit.

**Table 3 – Description of measuring factors for analysis of segmentation.**

Measuring factors	Formula	Range	Value for perfect segmentation
DSC[31]	$\frac{2 \times TP}{FP + (2 \times TP) + FN}$	0-1	1
ACC	$\frac{TP + TN}{TP + FP + TN + FN} \times 100$	0-100	100
SENS [31]	$\frac{TP}{TP + FN}$	0-1	1
OSeg [32]	$1 - \frac{area(x \cap y)}{area(x)}$	0-1	0
USeg [32]	$1 - \frac{area(x \cap y)}{area(y)}$	0-1	0

*x* = Ground Truth; *y* = Segmented output; *area*(*x*∩*y*) = TP;  
*area*(*x*) = total number of pixels with value 1 in *x*;  
*area*(*y*) = total number of pixels with value 1 in *y*.

ground truth data and decreases the accuracy of segmentation result.

Table 3 shows the formulation of all the measuring factors. Some of the measures may also give a better result for erroneous segmentation of a given image. So, the performance measure is quantified depending on all the measuring factors (as mentioned in Table 4) together for each segmentation technique.

The quantification of the RASIT method of segmentation and seven other states of the art methods and two newly published methods for segmentation were evaluated using the ground truth data. The state of the art threshold based segmentation techniques used for comparison are Otsu's multi-thresholding (Otsu) [33], Kapur's multi-thresholding (Kapur) [34] and Particle Swarm Optimization (PSO) based multi-thresholding techniques [21]. From the areas of cluster based segmentation, K-means [16-18], Fuzzy C-means (FCM) [2,15] and Expectation Maximization (EM) [2,19] based clustering methods are used for comparison.

The region growing [24,25] is also followed for state-of-the-art method based comparison. Beyond the state of the art method, the Fractional-Order Darwinian Particle Swarm Optimization (FODPSO) [35] and the Multilevel Thresholding-based Electro-Magnetism Optimization (MTEMO) [36] methods are also used for comparative study by following the theory of optimization. Apart from region growing, all

the other methods used for comparative study generate clustered output. The cluster number varies depending on the user input parameters. In our analysis, we generated nine different set of clustered output of all the existing methods (except region growing) by varying the input parameter (number of cluster/threshold number/threshold level) from 2 to 10. For each thermogram, the validity index is used to evolve the appropriate number of clusters from the nine sets of clustered outputs using cluster validity Index I [37]. Index I is used for the selection of appropriate clustered image comparing with the input image. The clustering techniques used in comparative study contains the limitation of cluster number selection for each input. So for minimization of the problem, we use Index I [37] based cluster number selection method here. This index is found to reach its maximum value when the appropriate number of clusters is achieved by comparing the input data and cluster output. In the post-processing step of existing methods (except region growing), the cluster containing the pixel with maximum intensity value is extracted and considered as the final segmented region. In the case of region growing, the best result is obtained by manual selection of seed points and by fixing the threshold value to 0.01 through trial and error method. The outputs of all the segmentation techniques used for the comparative study are converted into a binary image for analysis with ground truth data. Fig. 6

**Table 4 – Performance measure of RASIT method and comparison with existing techniques.**

Sl. no.	Used techniques	Knee thermogram dataset					DMR breast thermogram dataset				
		DSC	ACC (%)	SENS	OSeg	USeg	DSC	ACC (%)	SENS	OSeg	USeg
1	RASIT (proposed)	0.805	98.2	0.857	0.157	0.143	0.576	96.98	0.491	0.057	0.509
2	Otsu thresholding [12]	0.509	90.77	0.357	0	0.64	0.281	83.96	0.175	0	0.825
3	Kapur thresholding [12]	0.19	60.23	0.107	0	0.89	0.145	44.95	0.085	0	0.915
4	PSO [21]	0.285	76.71	0.169	0	0.83	0.141	63.47	0.082	0	0.918
5	K-means [16-18]	0.472	83.22	0.34	0	0.66	0.362	89.93	0.243	0	0.758
6	Fuzzy C-means [2,15]	0.54	92.06	0.388	0	0.61	0.412	92.1	0.283	0	0.717
7	Expectation maximization [2,19]	0.471	88.44	0.326	0	0.67	0.274	79.68	0.177	0.02	0.823
8	Region growing [24,25]	0.922	99.31	0.903	0.06	0.1	0.707	98.81	0.87	0.296	0.131
9	FODPSO [35]	0.318	79.02	0.195	0	0.81	0.144	64.27	0.084	0	0.917
10	MTEMO [36]	0.19	60.03	0.106	0	0.89	0.162	49.91	0.109	0.009	0.894

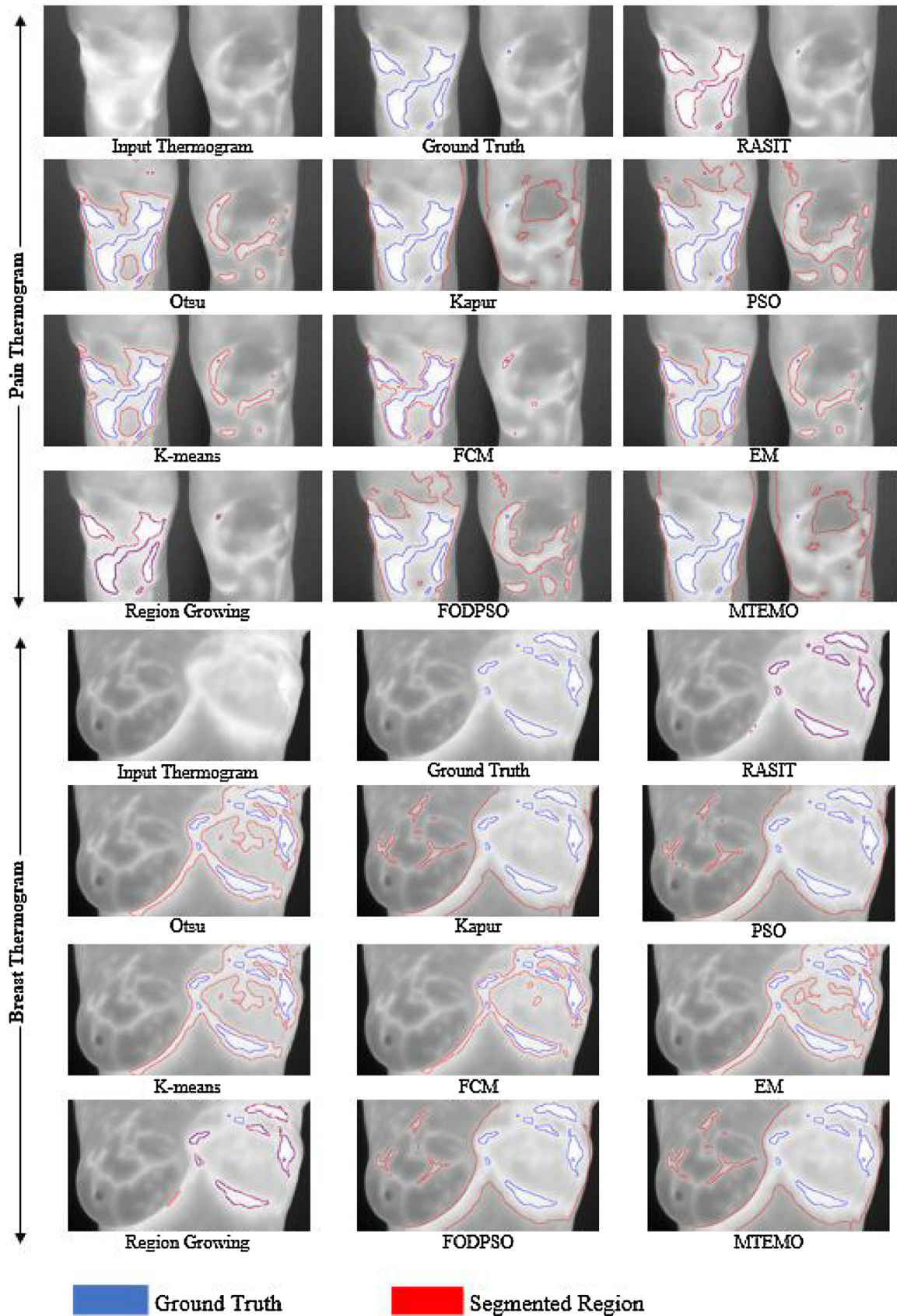


Fig. 6 – Thermogram segmentation outputs (blue border represents the ground truth and red border represents the segmented region by the mentioned methods). The captions given below of each image represents the input image/ground truth/name of the segmentation method.

illustrated the final segmented outcome of RASIT and the existing methods along with the ground truths.

From Table 4 and from Fig. 6, we can observe that except Region growing, the RASIT generates a better result, compared to the other state of the art methods in terms of DSC, ACC, SENS and USeg for both the pain and DMR breast thermogram dataset with a negligible increase in OSeg. However, the performance of Region Growing varies based on the selection of seed point(s) and the threshold value. Though region growing gives better result compared to the proposed RASIT method, the manual selection of seed point(s), and the threshold value are time-consuming and complicated task to perform.

### 5.2. Significance analysis of the performance measures

In order to evaluate the statistical significance of the obtained result, the Wilcoxon's nonparametric [36,38] test was performed over the measuring factors given in Table 4 by considering 1% significance level. The statistical test was conducted to judge whether the group-wise final result of the evaluation criteria (DSC, ACC, SENS, OSeg, USeg) acquired from the RASIT method statistically differ in a significant way from other existing methodologies of segmentation or not. The null hypothesis is considered if P-value is greater than or equal to 0.01 and indicates that there is no difference between two groups. On the other hand, if P-value is less than 0.01 then it is a strong evidence for rejecting the null hypothesis.

Observations from the analysis show that, the P-values of all the evaluation criteria for all the methods except region growing is less than at least by  $10^{-6}$  ( $P < 10^{-6}$ ), so it rejects the null hypothesis. Therefore, generated results by existing methods are group-wise different from RASIT method. However, the better performances of Region Growing depending on SENS, OSeg and USeg for pain thermogram and again SENS and OSeg for breast thermogram are group-wise similar compared to proposed RASIT method as the P values for those factors are greater than 0.01. Observations of Table 4 following the statistical analysis also shows that, the difference between the outcome of Region Growing and RASIT is negligible in case of Knee thermogram dataset depending on SENS, OSeg and USeg based performance measuring factors. It may also be observed that the differences between performance measur-

ing factors of RASIT and region growing is less for knee thermogram dataset compared to those of RASIT and other existing methods.

## 6. Discussions

Selection of the termination point of execution is an important part of RASIT method and determined by the value of  $\mu$ , as mentioned in Section 3. In the first part of this section, the issues related to the selection of  $\mu$  value is detailed. The rest of the section contains discussion about the advantages of the proposed RASIT method compared to other existing methods.

### 6.1. Sensitivity of $\mu$ value selection in RASIT method

In our proposed method (RASIT), an iteration stopping criteria ( $\mu$ ) is used to stop the iterative progress of RASIT. Selection of the  $\mu$  value as 0 will not terminate the execution of RASIT method as it will accept the null difference between threshold values generated automatically in two successive steps. The minimum value of  $\mu$ , i.e.,  $\mu = 1$ , extracts the region which shows the source of inflammation represented by the pixels having highest gray level or pixels with gray levels very close to the highest gray level within a range of small variance and which leads to the over-segmentation. However, in our analysis, we want to extract the whole area of inflammation spreading. It is observed that, in the Figs. 7 and 8, under segmentation increases proportionately with the increase of  $\mu$ -value. Therefore, the value of  $\mu$  is fixed to 2 to avoid both under and over segmentation and to extract the optimal inflamed region(s).

The effects of changes in the value of  $\mu$  for the present method over knee and breast thermogram datasets depending on measuring factors like Dice's similarity coefficient (DSC), Accuracy (ACC), Sensitivity (SENS), Over segmentation (OSeg), and Under segmentation (USeg) are shown in Figs. 7 and 8 respectively.

### 6.2. Advantages of the RASIT method

The proposed RASIT method minimizes the limitations of parameter selection, execution time complexity and under-segmentation of ROI-contained by existing techniques. This

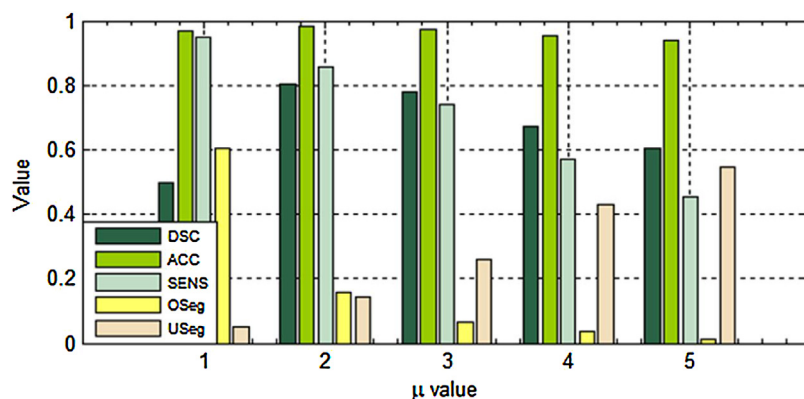


Fig. 7 – Performance measuring factors of Segmentation with different  $\mu$  values for Knee thermogram dataset.

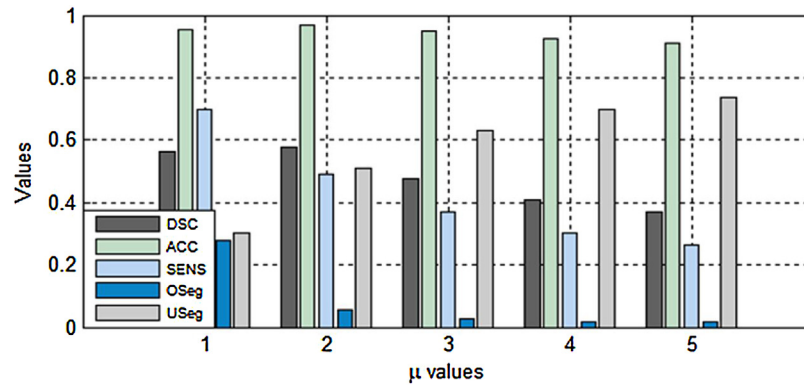


Fig. 8 – Performance measuring factors of Segmentation with different  $\mu$  values for Breast thermogram dataset.

section describes the advantages of RASIT method depending on the stated three limitation solving points as given in contribution part.

#### 6.2.1. Minimization of the complexity of parameter selection

The existing state of the art thermogram segmentation techniques suffer from the complexity of parameter selection as described in Table 1 of the paper. In the case of clustering technique, selection of optimal cluster number is a complex task. In our comparative study, we performed the index I [37] based analysis of clustered output of each thermogram for optimal cluster image and number selection from nine sets of clustered outputs as detailed in Section 5.1. The sets are generated by varying the cluster number from 2 to 10. Rather than cluster number selection, each of the existing methods contains limitation related to other parameter selection as given in Table 5. In our proposed method (RASIT), the complexity of parameter selection is minimized by fixing the iteration stopping criteria ( $\mu$ ) with value 2. Segmentation of the region related to spread of inflammation may be

performed with  $\mu$  value 2 for all types of medical infrared thermogram. In the case of the origin of the inflammation area extraction, the  $\mu$  value will be fixed to 1. Table 5, shows that except the Otsu and Kapur's multi-thresholding based segmentation technique, the proposed method needs a minimum number of user input compared to all other methods. Though the number of user input for Otsu and Kapur method is similar to our proposed method, but the accuracy of Otsu and Kapur methods are very much lower compared to RASIT method (shown in the Table 4).

#### 6.2.2. Minimization of execution time complexity

The time complexity of the proposed RASIT method is based on number of iterations required to reach termination condition, time for EFI generation for each iteration and size of the input image. Considering required number of iterations as  $T$ , size of the image as  $N$ , and the neighborhood window size of each pixel as  $w$ , the time complexity of RASIT method is  $O((wN)T)$ . In the comparative study, except region growing all the methods generates clustered output. The optical cluster is

Table 5 – Parameter details.

Segmentation techniques	Number of input parameters	Parameter description
RASIT	1	Iteration stopping criteria ( $\mu$ ).
Otsu	1	Number of threshold level.
Kapur	1	Number of threshold level.
PSO	6	Total number of iteration, global weights, local weights, initial number of particles within each swarm, inertial coefficient, and maximum number of levels a particle can travel between iterations.
K-means	2	Cluster number, Cluster center.
FCM	4	Cluster number, Cluster center, fuzzy weighting exponent, stopping condition.
EM	3	Cluster number, Data point initialization, stopping condition.
Region growing	2	Seed points, threshold value.
FODPSO	12	Total number of iteration, maximum stagnation of swarms, global and local weight, initial, minimum and maximum number of particles within each swarm, initial, minimum and maximum number of swarm, and maximum number of levels a particle can travel between iterations, fractional coefficient.
MTEMO	6	Total number of iteration, value of local search phase, distance of local search phase, population size, population initialization, number of threshold.

**Table 6 – Time complexity of each method.**

Used techniques	Method oriented time complexity	I-index time complexity	Time complexity of final cluster extraction
RASIT	$O((wN)T)$	Not required	Not required
Otsu	$O(L^n)$	$O(nN)$	$O(N)$
Kapur	$O(L^n)$	$O(nN)$	$O(N)$
PSO	$O(nN^p)$	$O(nN)$	$O(N)$
K-means	$O(NndT)$	$O(nN)$	$O(N)$
Fuzzy C-Means	$O(Nn^2dT)$	$O(nN)$	$O(N)$
Expectation maximization	$O(nk)$	$O(nN)$	$O(N)$
Region growing	$O(NT)$	Not required	Not required
FODPSO	$O(n\sum_{vs}N^s)$	$O(nN)$	$O(N)$

*N* = size of the image; *n* = threshold/cluster number; *T* = number of iteration; *w* = neighborhood window size; *L* = highest intensity level; *d* = number of dimension; *k* = number of hidden unit per vector; *v* = number of vectors; *N<sup>p</sup>* = number of particles within the population; *N<sup>s</sup>* = initial number of swarm within each swarm(s).

selected from a set of clustered output using Index I [37]. So the time complexity of index I is added with the original time complexity of each method. In our analysis, the time complexity of Index I is  $O(nN)$  where *n* is the cluster number and *N* is the size of the image. Also, in case of clustering method oriented outputs, the cluster representing the inflamed region need to be extract and binarization is required in the post processing step. Extraction of the cluster representing the inflamed region contains time complexity of  $O(N)$ . Here also the size of the image is *N*. Except RASIT and Region Growing, all the methods are executed for 9 times by changing the cluster/threshold number from 2 to 10. So the time complexity will multiplied by 9 for each method. For all the methods (except RASIT and region growing), the I index [37] time complexity and time complexity of final cluster extraction is added with the method's own time complexity. In Table 6, the time complexity of each method is given except MTEMO [36]. In case of MTEMO, the time complexity is not defined, but this method takes maximum time for execution (in seconds).

From Table 6 and the above discussion, we observed that Region Growing is the only algorithm that shows significant advantage in terms of computation complexity in comparison with the proposed method (RASIT). However Region Growing suffers from detrimental disadvantages of proper threshold and seed selection. Since the proposed method contains minimum complexity of user input, it should be a judicious choice for automatic thermal image segmentation with optimal accuracy.

**6.2.3. Minimization of under segmentation**

Under segmentation of inflamed region results increase amount of ROI extraction in the final segmentation output compared to the ground truth data. In thermogram segmentation, except Region Growing all the existing methods overcome the drawback of over segmentation which results in a large amount of under segmentation rate as shown in Table 4. Our proposed method (RASIT) minimizes the rate of under segmentation with negligible increase in over segmentation rate for both the breast and arthritis knee thermogram. With proper selection of seed points and the threshold value, region growing generates a minimum amount of over and under-segmentation rate. But the selection of accurate seed points is a complex task to

perform. Excluding region growing, the proposed RASIT method generates the lowest rate of under segmentation compared to all the techniques used for comparative study as shown in Table 4.

**7. Conclusion and future work**

Inflammation on the knee joint surface due to arthritis indicates the presence of certain abnormalities in the body defense system, which may lead to a permanent joint damage. On the other hand, asymmetric inflammation in breast region is a strong evidence of breast abnormality. Accurate segmentation of the inflamed ROI from thermograms assists in the quantification of the spread of inflammation and identifies the affected region accurately. The proposed RASIT method achieved the segmentation of the ROI with significant accuracy. Except region growing, the comparative study shows that the RASIT method achieved better performance compared to the state-of-the-art segmentation techniques. Although region growing generates best segmentation accuracy with a minimum rate of over and under-segmentation, but it requires manual identification of seed points and the threshold value for optimal performance rate. Besides that, RASIT decreases the complexity of parameter selection and amount of under-segmentation. Furthermore, the statistical test over the performance measures indicates that the RASIT method generates better results on all the thermograms in the dataset with a 99% confidence interval. In the expanded version of the RASIT method, the over-segmentation problem for knee thermograms will be tackled by the generation of image oriented automated iteration stopping criteria.

**Ethical approval**

The study was permitted by the Institutional Ethical Committee approval number F.4 (5-2)/AGMC/Academic/Project/ Research/2007/Sub-I/8199-8201, Dated: 18th November, 2013 for DBT project and approval number F.4 (5-196)/AGMC/Academic/Research Cell Meeting/2015, Dated: 24th January, 2018 for ICMR project.

## Acknowledgments

The second author would like to thank Dr. S.B. Nath, Assistant Professor and HOD (I/C), Agartala Government Medical College (AGMC), Agartala, Tripura, India for his support during the collection of knee thermogram dataset and Prof. Paramartha Dutta, Visva-Bharati, West Bengal, India for his helpful discussions during the finishing stages of this work. This work was supported by Department of Biotechnology (DBT), Government of India, of project Grant No. BT/533/NE/TBP/2013, Dated 03/03/2014 and Indian Council of Medical Research (ICMR), Government of India, under Grant Number. 5/7/1516/2016-RCH, Dated: 20/06/2017.

## REFERENCES

- [1] Bardhan S, Bhowmik MK, Nath S, Bhattacharjee D. A review on inflammatory pain detection in human body through infrared image analysis. International Symposium on Advanced Computing and Communication (ISACC) 2015. <http://dx.doi.org/10.1109/isacc.2015.7377350>
- [2] Snehalatha U, Anburajan M, Teena T, Venkatraman B, Menaka M, Raj B. Thermal image analysis and segmentation of hand in evaluation of rheumatoid arthritis. International Conference on Computer Communication and Informatics 2012. <http://dx.doi.org/10.1109/iccci.2012.6158784>
- [3] Ng E-K. A review of thermography as promising non-invasive detection modality for breast tumor. Int J Thermal Sci 2009;48:849-59. <http://dx.doi.org/10.1016/j.ijthermalsci.2008.06.015>
- [4] Etehadtavakol M, Chandran V, Ng E, Kafieh R. Breast cancer detection from thermal images using bispectral invariant features. Int J Thermal Sci 2013;69:21-36. <http://dx.doi.org/10.1016/j.ijthermalsci.2013.03.001>
- [5] Arthritis - National Library of Medicine - PubMed Health. National Center for Biotechnology Information. <https://www.ncbi.nlm.nih.gov/pubmedhealth/PMHT0024677/> [accessed 23.03.18].
- [6] World Arthritis Day | National Health Portal of India. [https://www.nhp.gov.in/World-Arthritis-Day\\_pg](https://www.nhp.gov.in/World-Arthritis-Day_pg) [accessed 23.03.18].
- [7] Nichols H. Arthritis: causes, types, and treatments. Med News Today 2017, <http://www.medicalnewstoday.com/articles/7621.php> [accessed 23.03.18].
- [8] Dieppe P. Epidemiology of the rheumatic diseases Second Edition. AJ Silman, MC Hochberg (eds). Oxford: Oxford University Press, 2001, pp. 377, £95.00. ISBN: 0192631497. Int J Epidemiol 2002;(31):1079-80. <http://dx.doi.org/10.1093/ije/31.5.1079-a>
- [9] Milind P, Sushila K. How to live with rheumatoid arthritis? Int Res J Pharm 2012;3(3):115-21.
- [10] Bhowmik MK, Bardhan S, Das K, Bhattacharjee D, Nath S. Pain related inflammation analysis using infrared images. Thermosense: thermal infrared applications XXXVIII 2016 2016. <http://dx.doi.org/10.1117/12.2223425>
- [11] Mital M, Scott EP. Thermal detection of embedded tumors using infrared imaging. J Biomech Eng 2007;129:33. <http://dx.doi.org/10.1115/1.2401181>
- [12] Jadin MS, Taib S. Infrared image enhancement and segmentation for extracting the thermal anomalies in electrical equipment. Electron Electr Eng 2012;120. <http://dx.doi.org/10.5755/j01.eee.120.4.1465>
- [13] Cong-Ping C, Wu Q, Zi-Fan F, Yi Z. Infrared image transition region extraction and segmentation based on local definition cluster complexity. International Conference on Computer Application and System Modeling (ICCASM) 2010. <http://dx.doi.org/10.1109/iccasm.2010.5620268>
- [14] Fan S, Yang S. Infrared electric image segmentation using fuzzy Renyi entropy and chaos differential evolution algorithm. International Conference on Future Computer Sciences and Application 2011. <http://dx.doi.org/10.1109/icfcsa.2011.57>
- [15] Araki S, Nomura H, Wakami N. Segmentation of thermal images using the fuzzy C-means algorithm. Proceedings of the Second IEEE International Conference on Fuzzy Systems 1993. <http://dx.doi.org/10.1109/fuzzy.1993.327400>
- [16] Golestani N, Etehad Tavakol M, Ng EYK. Level set method for segmentation of infrared breast thermograms. EXCLI J 2014;13:241.
- [17] Snehalatha U, Anburajan M, Sowmiya V, Venkatraman B, Menaka M. Automated hand thermal image segmentation and feature extraction in the evaluation of rheumatoid arthritis. Proc Inst Mech Eng H: J Eng Med 2015;229:319-31. <http://dx.doi.org/10.1177/0954411915580809>
- [18] Shahari S, Wakankar A. Color analysis of thermograms for breast cancer detection. International Conference on Industrial Instrumentation and Control (ICIC) 2015. <http://dx.doi.org/10.1109/iic.2015.7151001>
- [19] Ramirez-Rozo TJ, Garcia-Alvarez JC, Castellanos-Dominguez CG. Infrared thermal image segmentation using expectation-maximization-based clustering. XVII Symposium of Image Signal Processing and Artificial Vision (STSIVA) 2012. <http://dx.doi.org/10.1109/stsiva.2012.6340586>
- [20] Guofeng J, Wei Z, Zhengwei Y, Zhiyong H, Yuanjia S, Dongdong W, et al. Image segmentation of thermal waving inspection based on particle swarm optimization fuzzy clustering algorithm. Meas Sci Rev 2012;12. <http://dx.doi.org/10.2478/v10048-012-0041-6>
- [21] Sayed GI, Soliman M, Hassani AE. Bio-inspired swarm techniques for thermogram breast cancer detection. Med Imaging Clin Appl Stud Comput Intell 2016;487-506. [http://dx.doi.org/10.1007/978-3-319-33793-7\\_21](http://dx.doi.org/10.1007/978-3-319-33793-7_21)
- [22] Font-Aragones X, Faundez-Zanuy M, Mekyska J. Thermal hand image segmentation for biometric recognition. IEEE Aerospace Electron Syst Mag 2013;28:4-14. <http://dx.doi.org/10.1109/maes.2013.6533739>
- [23] Dutta T, Sil J, Chottopadhyay P. Condition monitoring of electrical equipment using thermal image processing. IEEE First International Conference on Control Measurement and Instrumentation (CMI) 2016. <http://dx.doi.org/10.1109/cmi.2016.7413761>
- [24] Selvarasu N, Vivek S, Nandhitha N. Performance evaluation of image processing algorithms for automatic detection and quantification of abnormality in medical thermograms. International Conference on Computational Intelligence and Multimedia Applications (ICCIMA) 2007. <http://dx.doi.org/10.1109/iccima.2007.216>
- [25] Nandhitha NM, Manoharan N, Rani BS, Venkataraman B, Sundaram PK, Raj B. Performance evaluation of hot spot extraction and quantification algorithms for on-line weld monitoring from weld thermographs. Automation and Robotics in Construction — Proceedings of the 24th International Symposium on Automation and Robotics in Construction 2007. <http://dx.doi.org/10.22260/isarc2007/0077>
- [26] Zhou Q, Li Z, Aggarwal JK. Boundary extraction in thermal images by edge map. Proceedings of the 2004 ACM

- Symposium on Applied Computing – SAC 04 2004.  
<http://dx.doi.org/10.1145/967900.967956>
- [27] Glaßer C, Reitwiesner C, Selivanov V. The shrinking property for NP and coNP. *Theor Comput Sci* 2011;412:853–64.  
<http://dx.doi.org/10.1016/j.tcs.2010.11.035>
- [28] Silva LF, Saade DCM, Sequeiros GO, Silva AC, Paiva AC, Bravo RS, et al. A new database for breast research with infrared image. *J Med Imaging Health Inform* 2014;4:92–100.  
<http://dx.doi.org/10.1166/jmihi.2014.1226>
- [29] Malik NA. *Textbook of oral and maxillofacial surgery*. 3rd edition. New Delhi: Jaypee; 2016, Chapter 2, pp. 15.
- [30] Oliver Earl, Ruiz Jaime, She Steven, Wang Jun. *The software architecture of the GIMP*; 2006.
- [31] Marsousi M, Plataniotis KN, Stergiopoulos S. An automated approach for kidney segmentation in three-dimensional ultrasound images. *IEEE J Biomed Health Inf* 2017;21:1079–94.  
<http://dx.doi.org/10.1109/jbhi.2016.2580040>
- [32] Belgiu M, Drăguț L. Comparing supervised and unsupervised multiresolution segmentation approaches for extracting buildings from very high resolution imagery. *ISPRS J Photogram Remote Sens* 2014;96:67–75.  
<http://dx.doi.org/10.1016/j.isprsjprs.2014.07.002>
- [33] Otsu N. A threshold selection method from gray-level histograms. *IEEE Trans Syst Man Cybern* 1979;9:62–6.  
<http://dx.doi.org/10.1109/tsmc.1979.4310076>
- [34] Kapur J, Sahoo P, Wong A. A new method for gray-level picture thresholding using the entropy of the histogram. *Comput Vis Graph Image Process* 1985;29(140).  
[http://dx.doi.org/10.1016/s0734-189x\(85\)90156-2](http://dx.doi.org/10.1016/s0734-189x(85)90156-2)
- [35] Ghamisi P, Couceiro MS, Martins FML, Benediktsson JA. Multilevel image segmentation based on fractional-order Darwinian particle swarm optimization. *IEEE Trans Geosci Remote Sens* 2014;52:2382–94.  
<http://dx.doi.org/10.1109/tgrs.2013.2260552>
- [36] Oliva D, Cuevas E, Pajares G, Zaldivar D, Osuna V. A multilevel thresholding algorithm using electromagnetism optimization. *Neurocomputing* 2014;139:357–81.  
<http://dx.doi.org/10.1016/j.neucom.2014.02.020>
- [37] Maulik U, Bandyopadhyay S. Performance evaluation of some clustering algorithms and validity indices. *IEEE Trans Pattern Anal Mach Intell* 2002;24:1650–4.  
<http://dx.doi.org/10.1109/tpami.2002.1114856>
- [38] Wilcoxon F. Individual comparisons by ranking methods. *Biometrics Bull* 1945;1:80.  
<http://dx.doi.org/10.2307/3001968>